Imaging Nanometer-Sized α-Synuclein Aggregates by Superresolution Fluorescence Localization Microscopy

M. Julia Roberti,[†‡] Jonas Fölling,[§] M. Soledad Celej,[‡] Mariano Bossi,[§] Thomas M. Jovin,[‡*] and Elizabeth A. Jares-Erijman[†]

[†]Departamento de Química Orgánica, Facultad de Ciencias Exactas y Naturales (FCEyN), Universidad de Buenos Aires, Ciudad Universitaria, Buenos Aires, Argentina; and [‡]Laboratory of Cellular Dynamics and [§]Department of Nanobiophotonics, Max Planck Institute for Biophysical Chemistry, Göttingen, Germany

ABSTRACT The morphological features of α-synuclein (AS) amyloid aggregation in vitro and in cells were elucidated at the nanoscale by far-field subdiffraction fluorescence localization microscopy. Labeling AS with rhodamine spiroamide probes allowed us to image AS fibrillar structures by fluorescence stochastic nanoscopy with an enhanced resolution at least 10-fold higher than that achieved with conventional, diffraction-limited techniques. The implementation of dual-color detection, combined with atomic force microscopy, revealed the propagation of individual fibrils in vitro. In cells, labeled protein appeared as amyloid aggregates of spheroidal morphology and subdiffraction sizes compatible with in vitro supramolecular intermediates perceived independently by atomic force microscopy and cryo-electron tomography. We estimated the number of monomeric protein units present in these minute structures. This approach is ideally suited for the investigation of the molecular mechanisms of amyloid formation both in vitro and in the cellular milieu.

INTRODUCTION

Protein aggregation is a key event in a number of human neuropathies characterized by the presence of amyloid structures in brain tissue, assembled from monomeric protein units aggregated into fibrils with a cross-β secondary structure (1). Among them, Parkinson's disease (PD) is the most common motor neurodegeneration and has been linked to the aggregation of α-synuclein (AS), a small (~15-kDa) presynaptic, natively unfolded protein (2). Amyloid aggregates of AS are found in the cytoplasm of dopaminergic neurons in the midbrain (substantia nigra) of individuals affected with PD, and the clinical symptoms of the disease correlate with neuronal loss. However, the complex, probably manifold, mechanisms responsible for cytotoxicity are yet to be elucidated (3,4). In vitro investigations have generally portrayed amyloid protein aggregation as a nucleation-polymerization process, according to which monomers first associate into oligomeric species (nucleation phase), which seed the formation of self-propagating mature amyloid fibrils (elongation phase) and their ultimate entangled aggregates (5). The most recent investigations on cells point to oligomers as the primary injurious species, acting to induce mitochondrial dysfunction, impair protein quality control, and interfere with synaptic function (4,6). The mature aggregates may actually play a neuroprotective role, i.e., by depleting the cellular milieu of the more dynamic, toxic intermediates (3).

The visualization in situ of oligomeric intermediates, and of amyloid structures in general, is fundamental to understanding the underlying mechanisms and factors that trigger and modulate the steps leading to fibrillation, and thus also to understanding the interplay between protein aggregation and loss of cellular homeostasis (7). The inherent nature of the targets poses technical difficulties. On the one hand, the AS oligomers described in the literature generally consist of structures $<$40 nm in size, although we have reported, in a parallel communication, the formation of supramolecular intermediates that approach 0.5 μm in diameter (8). In contrast, mature fibrils (prepared in vitro) are several μm long but only ~10 nm in diameter (9). The ultrastructure and morphological features of the AS amyloid species have been investigated at high resolution using atomic force microscopy (AFM) (9–11), electron microscopy (EM), and, most recently, cryo-electron tomography (cryo-ET) (8). These techniques are limited to the observation of surface topography, in the case of cells, and generally require fixation and sectioning (EM). The transient early stages of aggregation may be particularly susceptible to loss during the latter procedures.

In view of these considerations, different fluorescence microscopic techniques offer significant advantages for imaging aggregation reactions. Numerous probes have been developed for this purpose (12–16). In our own studies

Submitted August 29, 2011, and accepted for publication March 2, 2012.

*Correspondence: tjovin@gwdg.de

The corresponding author, Elizabeth A. Jares-Erijman, tragically died during the final revisions of this article. The surviving authors dedicate the article to her memory in acknowledgment of her passion for life and work, inspired leadership, and unfailing support.

M. Julia Roberti's present address is Cell Biology and Biophysics Unit, European Molecular Biology Laboratory, Heidelberg, Germany.

M. Soledad Celej's present address is Departamento de Química Biológica, CIQUIBIC-CONICET, Universidad Nacional de Córdoba, Córdoba, Argentina.

Mariano Bossi's present address is INQUIMAE-CONICET, Ciudad Universitaria, Buenos Aires, Argentina.

Editor: George Barisas.

0006-3495/12/04/1598/10 $2.00

doi: 10.1016/j.bpj.2012.03.010

of AS aggregation, we have relied on protein-bound small organic dyes and quantum dots for visualizing the location and state of the protein (17–22). Dynamic properties were assessed with the functional recombinant mutant AS (AS-C4) bearing a tetracysteine tag binding the fluorogenic biarsenical ligands FlAsH and ReAsH (22). In situ microscopy of molecular translational mobility using fluorescence recovery after photobleaching and of local molecular density using confocal fluorescence anisotropy (CFA) revealed a high mobility of free protein. In contrast, AS in larger aggregates was 80% immobile, whereas a small fraction with an apparent diffusion constant of ~0.04 mm^2/s was attributed to smaller, associated forms of AS-C4 and to exchange between mobile species and immobile aggregates. The spatial correlations between anisotropy and intensity also suggested the presence of small aggregates not detectable by conventional fluorescence imaging alone.

The main limitation of far-field fluorescence imaging, the finite spatial resolution imposed by the optical diffraction barrier (>~200 nm), has been overcome in recent years with the development of superresolution far-field fluorescence microscopies (23–25). A common principle shared by many of the currently employed strategies is the switching of a probe between dark (nonemitting) and bright (emitting) states. The switching either is performed at deterministic positions, with the spatial distribution of the probe controlled, as in the so-called targeted nanoscopies (e.g., STED, RESOLFT), or is allowed to occur at random positions, which are then computed precisely (to ~10–50 nm) in what is known as stochastic nanoscopy, or fluorescence localization microscopy (26–28), e.g., PALM, STORM, GSDIM, and variants thereof. In particular, the stochastic strategies such as PALM entail 1), random activation (switching on) of individual molecules; 2), registration of the emission signal in a wide-field image; 3), computational localization of the emission centroids, which can be accomplished with nanometer accuracy and precision to a degree dependent on the number of detected photons, dipole orientation, aberrations, and background; 4), depletion (by inherent photobleaching or photoreversal) of the observed molecules; and 5), repetition of steps 1–3 so as to randomly access another set of probe molecules. The superresolution image is generated from the cumulative spatial coordinates acquired in a large number of such cycles recorded in a long sequence of images.

The role of the fluorescent probe is crucial for achieving subdiffraction resolution in fluorescence localization microscopy (29). Most fluorescent markers used in single-molecule-switching-based nanoscopies can be classified into two main groups, photoswitchable fluorescent proteins and organic dyes. Although proteins have the unique advantage of being genetically encoded, they are not the most suitable choice for the study of AS aggregates. Previous reports suggest that fusion of a relatively large visible fluorescent protein (e.g., ~27 kDa for a GFP) to AS (14 kDa) can perturb the native properties of the amyloid protein (16,30). In contrast, organic dyes are much smaller than fluorescent proteins (typically 500–800 Da), and they usually have the additional advantage of being brighter and more photostable than photoswitchable proteins. Therefore, many efforts have been devoted to the synthesis of small organic molecules with controllable switching properties suitable for stochastic imaging approaches (31,32).

One family of rhodamine spiroamide (RSA) derivatives (33–35) was recently developed for single- or dual-color superresolution imaging (see Supporting Material). Upon exposure to ultraviolet (UV) light, these compounds exhibit the remarkable photophysical property of switching from a dark isomer to a fluorescent species through a ring-opening reaction of the five-member cycle containing the amide and the spirocarbon atom. The switching can be tuned by adjustment of the irradiance so that only a limited number of molecules are activated during each frame period, such that the corresponding emissions can be resolved without significant spatial overlap. RSAs offer some advantages over other organic probes used in superresolution microscopy. They display a simple and reliable switching mechanism that requires only low-intensity near-UV irradiation (~375 nm). In addition, proper switching of RSAs, unlike other markers used in similar techniques, does not rely on the presence of additional external chemical species such as oxygen scavengers (enzymes, polyvinyl alcohol), thiols, redox active species (e.g.. ascorbic acid, methyl viologen) (36), or a second nearby chromophore acting as a blinking facilitator (the activator) (37), which are not always compatible with the sample or the conditions of the experiment. Furthermore, these compounds have been derivatized with chemical groups that allow coupling with proteins or other biomolecules: *N*-hydroxysuccinimide ester (NHS) derivatives for primary amine groups and maleimide derivatives for selective reaction with thiols of cysteine-containing polypeptidic chains. In view of these properties, RSAs make suitable candidates for superresolution imaging of AS aggregation.

Here, we report the application of covalent labeling with RSA probes coupled with PALM microscopy in studies of AS amyloid aggregation both in vitro and in cells. We evaluated the suitability of various RSA dyes for labeling AS (AS-RSA) and optimized the aggregation conditions so as to maintain unaltered the morphology of the fibrillated structures, a condition assessed by AFM as a high-resolution reference technique. AS fibrils prepared in vitro were then imaged with subdiffraction fluorescence microscopy and the resolution enhancement was compared with that of conventional far-field microscopy and AFM. Furthermore, the dual labeling of AS was introduced as a means of monitoring the propagation phase of aggregation at distinct time points. Aggregation in cells was studied by microinjecting labeled AS, as in our previous reports based on a tetracysteine-biarsenical expression probe (17,19,21,22) in which the amyloid nature of the aggregates formed

was confirmed by confocal microscopy. We discerned the morphology of discrete, intracellular subdiffraction-size aggregates and generated estimates for the number of monomers involved in such structures.

MATERIALS AND METHODS

Protein labeling

AS was covalently labeled with compounds specifically developed for PALM applications at the Department of Nanobiophotonics, Max Planck Institute for Biophysical Chemistry, Göttingen, Germany. These compounds are derivatives of RSA and were chosen according to their emission properties and solubility in aqueous media. The selected compounds (Fig. S1 and Table S1 in the Supporting Material) were the sulfo-NHS derivative of RSA577 and the NHS derivative of RSA617, previously reported in multicolor imaging. The absorption maxima of the emitting open form are 570 nm and 600 nm, respectively, and the corresponding emission maxima are 577 nm and 617 nm. In addition, we labeled AS with the NHS derivative of the fluorescent Atto532 (ATTO-Tec, Siegen, Germany) for coinjection in AS aggregation assays within cells, to allow a quick visual reference for protein aggregation before superresolution imaging.

Protein labeling was carried out using standard amine-coupling techniques. Briefly, 1 ml of a 135 μM AS solution in 100 mM $NaHCO_3$ buffer, pH 8.3, was mixed with the NHS fluorophore derivative stock in a 1:3.5 protein/fluorophore molar ratio. The mixture was incubated at room temperature in an orbital stirrer for 1 h. The unbound dye was removed by size-exclusion chromatography using a PD10 column (Millipore, Billerica, MA), and the purified labeled protein was concentrated using a centrifugal device (molecular mass cutoff 3000 Da; Amicon, Millipore). The degree of labeling (DL), expressed as the number of fluorophore molecules/AS monomer, was estimated by absorbance measurements in a UV-visible spectrophotometer (Cary UV100, Varian, Palo Alto, CA), and yielded a DL of ~3 for AS-RSA577, AS-RSA617, and AS-Atto532 (estimated 10% error for DL).

Superresolution microscopy

Single- and dual-color image acquisition were performed with a laboratory instrument developed in the Nanobiophotonics Department. For dual-color acquisition, a beam splitter with a DM570 dichroic mirror (Chroma, McHenry, IL) was employed to separate the AS-RSA577 and AS-RSA617 emissions. For each sample, we acquired ~50,000–70,000 frames (acquisition time 10 ms/frame), and the image was reconstructed with a pixel size of 15 nm. The experimental setup (34), acquisition sequence, and image generation routine are described elsewhere (34,38). The image size was 12×12 μm for single-color images, and 10×5 μm for dual-color images. Image processing was then performed using MATLAB (The MathWorks, Natick, MA) and Imspector (Imspector Image Acquisition & Analysis Software, v0.1, http://www.imspector.de). For detailed information, see the Supporting Material.

Preparation of AS fibrils

For AS fibrillation, 400 μl of a 300 μM labeled AS solution in aggregation buffer (20 mM Tris-HCl, pH 7.7, 100 mM NaCl, and 0.02% NaN_3) were placed in 1.5-ml Eppendorf tubes and incubated overnight at 70°C with continuous agitation (350 rpm, Eppendorf Thermomixer, Eppendorf, New York, NY). The labeled/unlabeled AS molar ratio was 1:3. Fibril purification was carried out by removing a 50-μl aliquot of the aggregation mixture, placing it in a 1.5 ml Eppendorf tube, and centrifuging in a table top centrifuge (Eppendorf) at 13,000 rcf for 15 min. The supernatant was discarded, and the pellet containing the fibrils was resuspended in 100 μl aggregation buffer. The centrifugation/resuspension cycle was repeated twice. The final pellet was resuspended in 50 μl aggregation buffer/1% PVA, and the fibrils were subsequently deposited onto a glass coverslip as a thin film using home-built spin coater (conditions: 15 μl sample, 7000 rpm, 2 min).

The double-labeled AS fibrils for the elongation experiments with dual-color PALM detection were prepared by coincubating a 400-μl AS-RSA577 fibril suspension (equivalent monomeric AS concentration, 30 μM) with 50 μM monomeric AS-RSA617 using the same conditions described above supplemented with 500 μM spermine to accelerate aggregation. Fifty-microliter aliquots were removed at 30, 60, 180, and 360 min, purified, and mounted onto glass coverslips as described above. As a control, a sample of fibrils was prepared by incubating monomeric AS-RSA577, AS-RSA617, and unlabeled AS in a 1:1:6 molar ratio. In addition, the samples were also subjected to SDS denaturation by incubating the aliquots with 3 mM SDS at 95°C for 5 min before the purification routine.

Image analysis of AS distribution in two-color labeled fibrils

The distribution of AS-RSA617 monomer along preformed AS-RSA577 fibrils was carried out as follows. A binary mask was defined for each fibril and superimposed to the intensity image in the RSA577 and RSA617 channel. The corresponding intensities arising from the counts of single molecules detected in each channel (I_{577} and I_{617}, respectively) and percentile signal of each channel compared to the total single molecules count were estimated. In the experimental setup, the signal from RSA577 contributed to the signal in the RSA617 channel; this cross talk, estimated as a 10% of the signal measured in the RSA577 channel, was used to correct the RSA617 signal.

Real-time AS elongation observed by AFM microscopy

AFM imaging was performed using a Nanoscope IIIa microscope (Digital Instruments, Santa Barbara, CA) with a liquid cell coupled to a home-built temperature controller. A 90-μl sample containing purified AS fibrils in aggregation buffer was placed on a freshly cleaved mica surface, and 10 μl of a 50 μM monomeric AS + 500 μM spermine solution was added. The working temperature was adjusted to 45°C and images were acquired by continuous scanning in tapping mode (acquisition time 2 min). Image analysis was performed using the instrument software.

Characterization of intracellular AS aggregates

HeLa cells were cultured on glass coverslips (Menzel, Germany) in Dulbecco's modified Eagle's medium containing 4.5 g/l glucose, 10% fetal calf serum, and 1% penicillin/streptomycin (complete medium). The experiments were carried out by microinjecting monomeric AS into the cell cytoplasm, as reported earlier (17), using a semiautomatic microinjection apparatus and Femtotips (Eppendorf). The stock solution consisted of a mixture of AS-RSA577 and wild-type AS in a 1:3 molar ratio (total protein concentration 100 μM). RSA577 is not fluorescent until irradiated; thus, a small amount of AS labeled with the fluorescent dye Atto532-NHS (AS-Atto532) was included in the stock solution to detect the occurrence of aggregates by conventional confocal microscopy (Zeiss LSM 510 confocal microscope, Zeiss, Germany) before performing the superresolution imaging experiments (final AS-Atto532 concentration in the stock solution, 5 μM; laser line excitation, 532 nm). The intracellular protein concentration was estimated by assuming a 10-fold dilution of the microinjected protein stock solution (24). The initial distribution of protein, monitored by AS-Atto532 fluorescence, was homogeneous, but at 48 h, bright aggregates were evident in the cytoplasm and perinuclear region. At that point, the cells were fixed in 4% phosphate-buffered saline/paraformaldehyde, mounted in Mowiol (Kuraray America, Pasadena, TX), and then imaged. The diameter of aggregates was estimated using Imspector

by plotting the normalized intensity profiles and measuring the corresponding full width at half-maximum (FWHM) (sample set, $n > 20$). The aggregates with diameters <40 nm were classified as subdiffraction small aggregates (diameter estimated for oligomeric species of AS), and the aggregates with diameters between 40 nm and the confocal resolution were classified as medium-sized aggregates.

In addition, thioflavin S (ThioS) staining was performed to check the amyloid nature of the aggregates. To that end, cell samples prepared in parallel with those to be examined by superresolution imaging, were fixed with PFA 4% and stained using standard protocols for ThioS. Colocalization images of AS-Atto532 and ThioS were acquired with the confocal microscope. Atto532 was imaged using the DPSS 532 nm laser line for excitation, and ThioS images were acquired by exciting the probe with the 457-nm Ar-ion laser line.

Quantitative analysis of the number of AS molecules (m_{AS}) in subdiffraction-sized intracellular aggregates

Image processing was performed with Imspector and DIPImage. We defined masks for the aggregates (isodata masks from DIPImage), and measured the number of single molecules present, assuming that it should correspond closely to the AS monomers in view of the DL of ~3 and the labeled AS/unlabeled AS molar ratio of 1:3 for the microinjected solution. The m_{AS} values for small aggregates were plotted as a histogram. From the m_{AS} values of medium-sized aggregates, the associated volume (V_{agg}) was estimated assuming a spheroidal shape and the corresponding diameter values estimated from the FWHM measurements. The differences between the means of the diameters of the different batches of AS fibrils were subjected to statistical evaluation with unpaired, two-tailed Student's t-tests. Data are reported as the mean ± SE, with sample set sizes of $n > 20$ and $P < 0.05$.

RESULTS AND DISCUSSION

Fluorescence labeling and superresolution imaging of AS fibrils in vitro

We first characterized the features of amyloid structures prepared in vitro (Fig. 1). We tested the optimal conditions for labeling AS with the NHS derivatives of rhodamine spiroamides RSA577 and RSA617 (34). The photophysical properties of these probes are well characterized and their suitability in two-color imaging experiments has been established by standard immunolabeling of cellular structures (see Materials and Methods and Supporting Material).

As indicated above, the probe size is a critical issue when evaluating suitability for labeling the small (140-aa) AS molecule. Therefore, we first assayed different AS-RSA labeling conditions for the monomeric protein (see Materials and Methods for details), profiting from the chemical reactivity of the side-group amines of lysines present in AS toward NHS derivatives of the RSA probes. Of the 15 lysines that constitute the AS primary sequence, 11 are located in the N-terminus of the protein, which is excluded from the fibril core upon aggregation (39). We minimized the potential perturbation of the AS aggregation properties by reducing the RSA labeling ratio. From imaging experiments of the purified AS monomers deposited on PVA films, we determined that a ratio of 1:3 in the final product, i.e., the labeled monomeric AS, maintained image quality and preserved the structural integrity of AS. Thus, while the localization of either 1:1 or 1:2 AS/RSA labeled monomers was very difficult and produced very poor-quality images, the 1:3 labeled monomers were adequately localized after data acquisition and processing. Protein overlabeling (i.e., a 1:10 labeled monomer) led to the precipitation of AS during sample workup (data not shown). All of the imaging experiments presented in the following sections were performed with the 1:3 amino-labeled protein, hereafter referred to as AS-RSA577.

AS-RSA577 was subjected to aggregation experiments to obtain labeled fibrils. It was necessary to coincubate with unlabeled AS to obtain fibrils with normal morphology (i.e., that of wild-type AS) while maintaining a sufficient

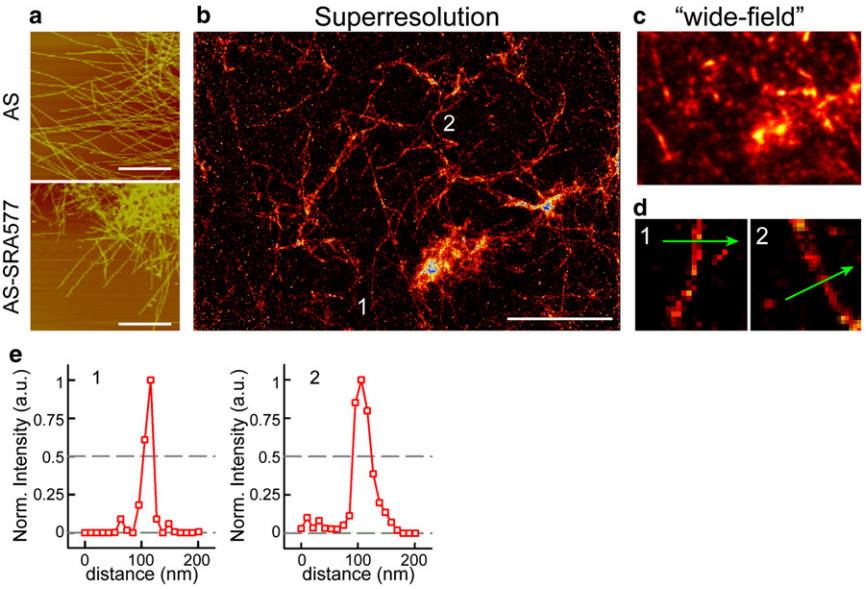

FIGURE 1 Superresolution imaging of AS fibrils prepared in vitro. (*a*) AFM images (height) of wild-type AS fibrils (*upper*) and AS-RSA577 fibrils (*lower*) acquired in tapping mode. Scale bar, 2.5 μm. (*b*) Superresolution image of AS fibrils and aggregates prepared from monomeric AS-RSA577. Scale bar, 2.5 μm; pixel size, 15 nm. (*c*) The corresponding wide-field image was generated by superposing the acquired frames without running any localization routine (same scale bar). (*d*) The diameter of the fibrils was estimated from the intensity profile across the fibrils (*green arrows*) for superresolution images of two selected fibrils. (*e*) Normalized intensity signal across the fibrils highlighted in *d*. A mean diameter of 24 ± 4 nm was extracted from the FWHM data (>20 fibrils measured).

content of dye to obtain meaningful images (see Materials and Methods). With the optimal AS-RSA577/wild-type AS labeling ratio of 1:3, the labeled fibrils had lengths and diameters comparable to those of the unlabeled fibrils (mean diameters by AFM, 9 ± 2.1 nm and 9 ± 1.8 nm, respectively, $n > 10$) (Fig. 1 *a*). The AS-RSA577 fibrils were purified and mounted in thin PVA films for fluorescence imaging. To focus the sample, the films were briefly irradiated at 375 nm to generate a small population of the probes in the emissive state. We acquired a sequence of ~50,000 frames (10 ms exposure time per frame) with an excitation power at 532 nm of 18 kW cm^{-2} in the focal plane. The first 100–1000 images were measured without photoinduced activation, i.e., by using the few spontaneously activated molecules. We then increased the dose of the activating light as the number of remaining markers decreased. The localization routine was applied to produce the final image, and an associated synthetic wide-field image was also created by superposing the raw frames (Fig. 1, *b* and *c*). The subdiffraction images revealed an intricate net of well-resolved fibrils in the entire field of view and it was also possible to identify fibrils within the aggregates. In contrast, the corresponding wide-field images lacked both sharpness and resolution power. The diameter of the fibrils spanned ≤ 2 pixels (pixel size, 15 nm) (Fig. 1 *d*). To quantify the improvement in lateral resolution (Δr), we plotted the normalized intensity profiles across the fibrils in the subdiffraction images, measured the corresponding FWHM values (Fig. 1 *e*), and referred the calculated mean to the theoretical value according to Abbe's limit ($\Delta r \sim \lambda/2$ NA). The mean diameter was 24 ± 4 nm ($n > 20$), which represented an improvement in lateral resolution, Δr, to ~$\lambda/10$. We attribute the enhancement in resolution to 1), the high number of RSA577 emitted photons, 2), the contrast between the emitting isomers and those in the obscure state, and 3), the reliable control of the switching of the fluorescent probes. The observed difference between the diameters estimated by AFM (~9 nm) and those estimated by PALM (~24 nm) reflects the resolution attainable with each technique.

We also carried out imaging experiments using AS-RSA617, a monomer labeled with a rhodamine spiroamide emitting at longer wavelengths than RSA577. The features of AS-RSA617 fibrils were comparable to those obtained with AS-RSA577 (data not shown).

Assessing in vitro fibril elongation with two-color subdiffraction fluorescence imaging

The successful implementation of AS labeling with a pair of dyes suitable for two-color imaging (RSA577 and RSA617) led to experiments of aggregation with both labels simultaneously, with the aim of characterizing the interaction between monomeric and fibrillated AS and the behavior of monomers during the elongation phase of the fibrils.

We had previously assessed in vitro fibril growth by means of AFM imaging in solution (Fig. S2). Preformed AS fibrils were deposited on a mica surface and incubated with an excess of monomeric AS so as to shift the chemical equilibrium toward fibril growth in the presence of 500 μM spermine, a compound known to accelerate AS aggregation (40,41). The elongation of the fibrils under the assay conditions was assessed by scanning the surface at 2-min intervals. After a brief lag time, the fibrils increased in length, with an average linear elongation rate of ~2 ± 1 nm/min (Fig. S2). Superresolution microscopy allowed the exploitation of the selectivity of fluorescence combined with the ability to distinguish in situ preexisting monomer units in the fibrils from those incorporated during the propagation phase. Color separation was established using PVA films containing monomeric AS separately labeled with RSA577 (*green channel*) or RSA617 (*red channel*). There was an ~10% cross-talk signal from RSA577 in the red channel, but no signal from RSA617 was detected in the green channel. We also prepared AS fibrils containing equimolar amounts of monomeric AS-RSA577 and AS-RSA617 to confirm that there was no preference for the inclusion of either monomer in the amyloid structure. To that end, we acquired images (Fig. S3), defined appropriate binary masks for the regions delimiting the fibrils, and estimated the percentage distribution of the total fluorescence signals in the two channels. Each channel contributed ~50% to the total fluorescence, in agreement with a random incorporation (i.e., independent of dye identity) of the labeled protein into the fibril. Furthermore, the dual-color images presented features indistinguishable from those obtained with single-color labeling; the fibrils were several μm in length and had diameters of ~20–30 nm.

For the fibril elongation experiments, we incubated AS-RSA577 fibrils with monomeric AS-RSA617 in the presence of 500 μM spermine (utilized in earlier AFM experiments). We removed samples at 0, 30, 60, 180, and 360 min, purified the fibrils to eliminate excess AS-RSA617, and imaged the fibrils mounted into thin PVA films (Fig. 2). At $t = 0$ min (green fibrils and red monomer were mixed for <1 min and then purified), the fluorescence signal of the fibrils was detected exclusively in the green channel (after correcting for cross talk), indicating the presence of only RSA577 (Fig. 2 *b*) and ruling out a fast, unspecific adsorption of free AS-RSA617 monomers onto the amyloid structure. In contrast, a significant contribution of AS-RSA617 was detected in the rest of the examined samples (Fig. 2, *c–f*). To quantify this observation, we segmented the images to define masks for the fibrils and estimated the fractional distribution of each dye (Table 1). The signal corresponding to AS-RSA617 was ~40% in all cases, and the label was evenly distributed along the fibrillar structure. This contribution did not disappear after incubating the samples with SDS, which reportedly dissociates AS fibrils at >2 mM concentration (42), suggesting the

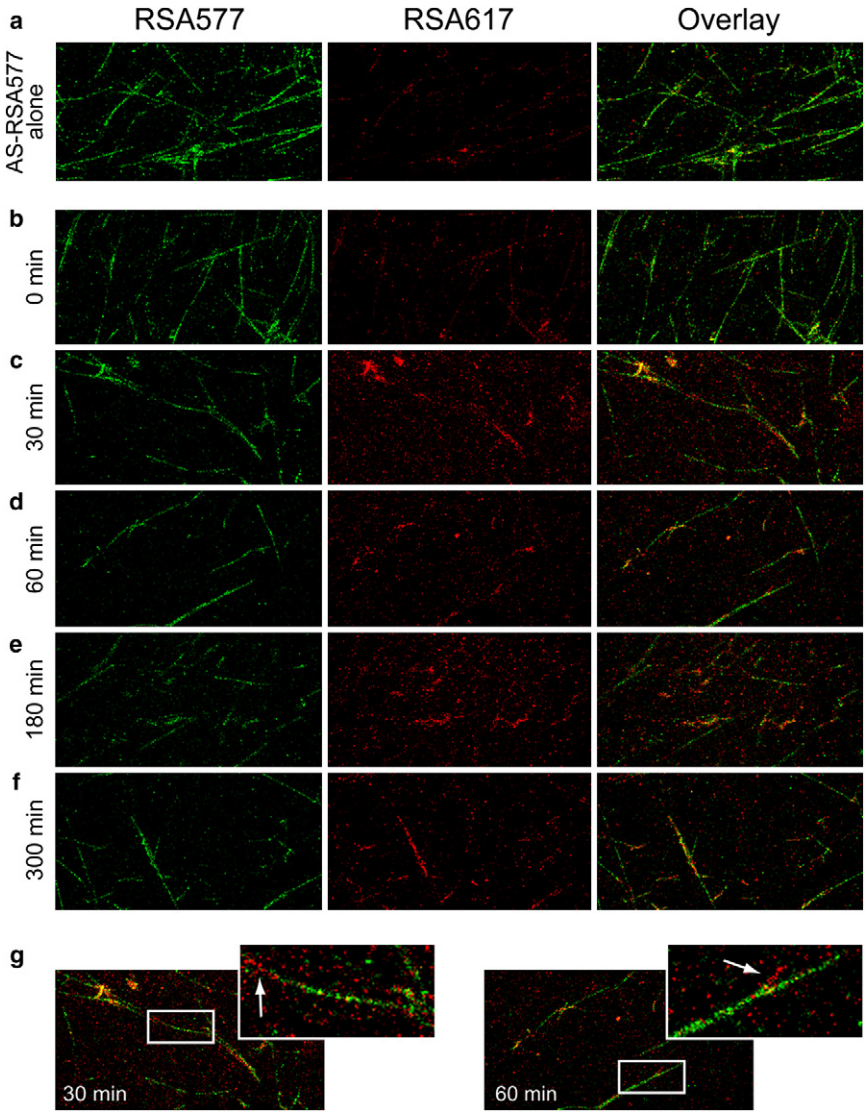

FIGURE 2 Two-color imaging of AS fibril elongation in vitro. (*a*) AS fibrils labeled with RSA577 observed by two-color superresolution imaging before mixing with AS-RSA617 monomer. Samples containing the preformed AS-RSA577 fibrils were then incubated with monomeric AS-RSA617 (*red*). (*b–f*) Aliquots were withdrawn at t = 0 (*b*), 30 (*c*), 60 (*d*), 180 (*e*), and 300 min (*f*) and imaged using a two-channel detection array. Left column (green), RSA577 channel; center column (red), RSA617 channel; right column, channel overlay. Scale bar, 2.5 μm. (*g*) Detail of fibril growth in samples corresponding to t = 30 (*left*) and 60 (*right*) min. Scale bar for insets, 3× magnification of original image.

occurrence of interactions or interchange mechanisms between AS in solution and fibrils. Furthermore, close inspection of the images revealed the presence of anchor points from which fibrils propagated from a preexisting structure (Fig. 2 *g*). These extensions were formed almost exclusively by AS-RSA617 monomers (>90% of the secondary fibrillar segments were assigned to the red channel). A noteworthy observation is that growth was unidirectional, i.e., the fibrils elongated only from one end of the structure, a feature previously described for the growth of amyloid Aβ peptide fibrils (43). From the length of the fibrils originating from the anchor points, we estimated a fibril growth rate of ~7 ± 4 nm/min.

TABLE 1 Fractional distribution of AS-RSA577 and AS-RSA617 signals in AS fibril elongation imaging assays

Sample	% AS-RSA577	% AS-RSA617
AS-RSA577 alone	90 ± 2	10 ± 2
0 min	93 ± 1	7 ± 1
30 min	42 ± 3	58 ± 3
60 min	41 ± 3	59 ± 3
180 min	41 ± 3	59 ± 3
300 min	48 ± 4	52 ± 4

Subdiffraction imaging of intracellular aggregates

The improvement in resolution observed in the experiments performed in vitro led us to a corresponding study of AS aggregation in cells. To that end, we microinjected AS-RSA577 mixed with wild-type AS in a 1:3 molar ratio (total protein concentration 100 μM) into HeLa cells and incubated them for 48 h at 37°C. Due to the lack of fluorescence of the closed form of AS-RSA577, we coinjected a small amount (~5 μM) of AS labeled with Atto532 (AS-Atto532) to monitor the occurrence of aggregates using

confocal microscopy. Aggregation proceeded with the development of spheroidal, perinuclear, highly fluorescent aggregated structures (Fig. 3 *a*), as we previously reported using a tetracysteine expression tag for AS (17,19,21,22). The amyloid nature of the aggregates was confirmed by ThioS staining of cell samples prepared in parallel (data not shown), since ThioS is a dye specific for the identification of amyloid structures in tissue. We distinguished two types of aggregates according to size—micrometer-sized aggregates, with diameters on the order of micrometers, and subdiffraction-sized aggregates, with apparent diameters close to the confocal resolution (~200 nm), which could not be resolved by conventional imaging. Once protein aggregation was confirmed, the cells were fixed and mounted. Superresolution images were acquired after the Atto532 was completely bleached.

We focused our attention on the subdiffraction aggregates in view of their potential cytotoxicity. They appeared similar by conventional far-field microscopy. The probe activation conditions yielded a distribution of single-molecule events sufficiently sparse for good imaging. In the case of the large, micrometer-sized aggregates, the probe density was excessive, such that it was not possible to activate and excite single molecules as required by the stochastic principle. Therefore, such large aggregates were not imaged under superresolution conditions. However, in contrast to previous reports of in vitro studies (8,10), we did not observe single fibrils emerging from such aggregates. Had fibrils with features similar to those seen in vitro (i.e., appreciable in length) been present, they would have been discerned due to the lower local concentration of dye in individual fibrils as displayed in our superresolution in vitro assays.

The resolution of our setup allowed us to perceive the subdiffraction-sized aggregates with a resolution of ~15 nm (Fig. 3, *b* and *c*). The structures were round in shape and were assigned to two distinctive subgroups based on size: subdiffraction small aggregates with diameters of <40 nm, and subdiffraction medium-sized aggregates with diameters in the range 40–200 nm, estimated from FWHM intensity profile measurements (Fig. 3, *d* and *e*). These two distinct types of structure bore striking resemblance to some of the nonamyloid (i.e prefibrillar) supramolecular colloidal species our laboratories and colleagues have recently observed in vitro using AFM and cryo-ET (8). These include early colloidal supramolecular associates (fuzzy balls) with an apparent diameter of ~30 nm, and the acunas (amyloid + cuna, the Spanish word for cradle) with diameters of up to 200–600 nm.

To further characterize these detected structures, we exploited the underlying principle of single-molecule localization to estimate the number of AS units (m_{AS}) in the subdiffraction structures. Our calculations involved the following conditions: 1), a 1:3 mixture of AS-RSA577/unlabeled (i.e., wild-type) AS was microinjected; 2), the DL of AS was ~3; and 3), the distribution of labeled markers within the aggregates was random. It is important

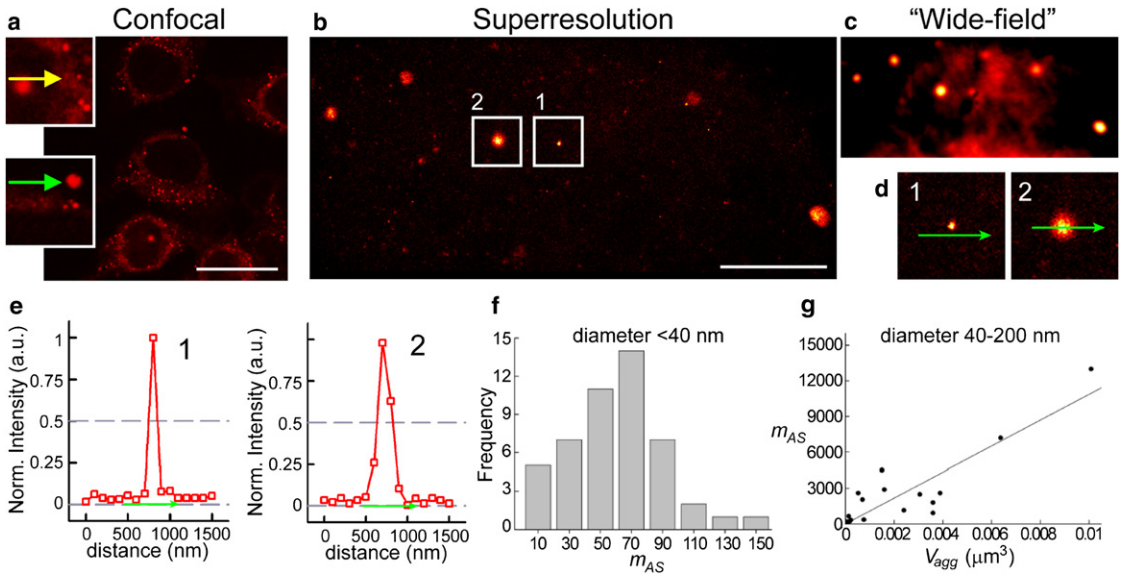

FIGURE 3 Characterization of intracellular subdiffraction-size AS aggregates. (*a*) Conventional confocal image of HeLa cells microinjected with a mixture of monomeric AS-Atto532, AS-RSA577 (nonfluorescent under the imaging conditions), and wild-type AS. Scale bar, 25 μm. (*Insets*) Detailed views of the presence of subdiffraction-sized (*yellow arrow*) and micrometer-sized (*green arrow*) aggregates. Scale bar, 4× magnification of original image. (*b* and *c*) Subdiffraction resolution image of aggregated AS in a cytoplasmic region of the cell (*b*) and the corresponding wide-field image (*c*). Scale bar, 2.5 μm, pixel size, 15 nm. (*d*) Detailed view of a subdiffraction small aggregate (diameter <40 nm) (*left*) and a subdiffraction medium-sized aggregate (diameter 40–200 nm) (*right*) extracted from *b*. Scale bar, 4× magnification of original image. (*e*) Normalized intensity profiles corresponding to the aggregates depicted in *d*. (*f*) Histogram of the number of AS monomers (m_{AS}) in small aggregates. (*g*) Correlation between m_{AS} and the corresponding volume of subdiffraction medium-sized aggregates. Linear fit to the data ($R^2 = 0.85$).

to point out that the dimensions are probably underestimated, partly because not all labeled molecules would have been activated, and also because some of the activated molecules may have been discarded in the thresholding step of the localization routine (26,34,38). The analysis resulted in an estimated m_{AS} of <100 AS monomers in the small aggregates. The histogram of m_{AS} values was centered at ~70 monomers/aggregate (Fig. 3 *f*). These results are compatible with descriptions of transient intracellular AS oligomers (see above) but using calculations based exclusively on indirect determinations in vitro (8), as in the case of the aforementioned fuzzy balls. In contrast, the medium-sized aggregates contained hundreds and even thousands of AS units, and are most probably correlated with the higher-order structures, the acunas. From the experimental data, we infer a roughly linear correlation between the number of AS monomers and the calculated volume of the aggregates (V_{agg}) (Fig. 3 *g*), assuming the accuracy of the diameter estimations and a spheroidal shape. In the event that the activation/detection efficiency in the axial direction over the range of particle dimensions was constant under our experimental conditions, such that all molecules were detected with equal probability, we can estimate from the data a volume/aggregated AS monomer of ~500–900 nm^3 (Fig. 3, *f* and *g*). A hydrodynamic radius of ~3 nm for partially compacted AS monomers would correspond to a value of ~110 nm^3. We tentatively conclude that during the presumed colloidal phase of AS association, AS maintains a constant but relatively low mean density consistent with the heterogeneous supramolecular nanostructures revealed by cryo-ET in vitro (8).

CONCLUSIONS

The experiments featured in this report offer promising perspectives for the investigation of the molecular mechanisms of amyloid formation both in vitro and in the cellular milieu. By using AS covalently functionalized with the selected dyes, we obtained labeled fibrils that conserved the morphology of those prepared from unlabeled protein. Direct labeling of AS offers an additional advantage compared to the use of immunofluorescence, considering the small size of both the monomeric protein and the amyloid structures. As an example, according to fluorescence nanoscopy experiments on cells stained with a tubulin-targeted primary antibody and a fluorescently labeled secondary antibody, the diameter of tubulin fibrils is ~70 nm, compared to ~30 nm reported by EM (44). The 70-nm value reflects the contribution of the diameter of the fibril and that of the bulky biomolecules employed for immunostaining. Superresolution microscopy reveals more accurately the size of the structure of interest. In vitro, we achieved a Δr of ~10 times below the classical limit. The diameters of the amyloid fibrils were estimated at ~20–30 nm, and it was possible to visualize individual fibrils within the dense aggregates. The double labeling experiments revealed terminal elongation of preexisting fibrils and initiation of branches from internal anchor points. These findings are in agreement with observations made by AFM imaging for the amyloid Aβ peptide (45), and the complementary data provide what to our knowledge are new insights into the kinetics and mechanistic aspects of fibril elongation. The elongation rate determined from the propagation experiments with the fluorescently labeled AS was in good agreement with that estimated by AFM. The value from the superresolution images has a higher uncertainty due to the fact that the measurements were not recorded continuously (as by AFM). We also detected the adsorption of freshly added monomer along the entire extent of resolved fibrils, indicating the existence of an exchange mechanism between fibrillated and free AS under the conditions of incubation, attesting further to the dynamic nature of the system.

It is possible to adapt and extend the assay to the study of AS interactions with other proteins and to the effects of agents promoting or inhibiting aggregation. Multicolor labeling also facilitates the detection of intermediate species involved in the aggregation process but invisible with ultraresolution techniques such as AFM and EM. Other amyloid proteins have been studied previously with total internal reflection fluorescence (TIRF) microscopy (46) using ThioT as the fluorescent label, but the approach is limited because ThioT is easily photobleached and exhibits fluorescence only at the stage of fibrillation; in addition, the lateral TIRF resolution is that of conventional fluorescence microscopy. The superresolution technique combined with TIRF achieves improvements in both lateral and axial resolution, as demonstrated in a recent study of intermediate and fibrillated stages of the Alzheimer's-disease-related Aβ peptide in vitro and within cells (47). In another report, the combination of AFM and fluorescence blink microscopy elucidated structural features of Huntingtin protein aggregates (48).

The experiments with cells revealed for the first time fluorescence images of discrete, small spheroidal structures that characterize the early stages of AS aggregation. The apparent diameter of such species when using conventional fluorescence microscopy is ~200 nm, compared to ~40 nm using PALM. Previous reports of AS oligomers in the cellular context provided only indirect evidence for such species. These investigations were based on AFM and EM microscopy of in vitro preparations and the analysis of cellular lysates by chromatography (49,50). The dimensions of the small spheroids visualized by superresolution microscopy are in good agreement with the estimates of ~24–34 nm using EM (49). However, a more compelling correlation is between the subdiffraction small and medium-sized aggregates and the supramolecular structures, fuzzy balls and acunas, recently discerned by combined AFM and cryo-ET. Under the proposed sequential association scheme

for AS colloidal intermediates (8,51), nonamyloid structures result from an initial condensation of monomeric or paucioligomeric AS. They subsequently collapse into thermodynamically more stable supramolecular assemblies with the unique capacity for promoting the formation of linear catenations maturing to the classical amyloid fibrils featured in Figs. 1 and 2. It is important to note that with the exception of Lewy bodies, there are no reports in the literature of the presence of canonical AS amyloid fibrils within mammalian cells; AS aggregates rather appear as punctuate inclusions (52–54) similar to those presented in this study.

In view of the constant development of fluorescence nanoscopies, we anticipate significant further improvements in achievable resolution and acquisition speed (55), enabling the monitoring of aggregation and structural transitions in real time and in living cells. In the latter case, fluorescent expression systems are required that can fulfill the dual requirements of preservation of AS molecular integrity and suitability for the superresolution microscopies. One possibility lies in the development of more photostable fluorogenic biarsenical compounds for use with the tetracysteine AS expression system (56).

SUPPORTING MATERIAL

Detailed description of the experimental setup, superresolution imaging acquisition, fluorescent markers, and three figures are available at http://www.biophysj.org/biophysj/supplemental/S0006-3495(12)00292-5.

We are thankful to Stefan Hell for providing the technical facilities for this investigation. The rhodamine spiroamides were kindly provided by Vladimir Belov. We also thank Christian Eggeling and Andreas Schönle for their assistance and fruitful discussions. E.A.J.-E. thanks the Max Planck Society (Partner Group grant), Agencia Nacional de Promoción Científica y Tecnológica, Consejo Nacional de Investigaciones Científicas y Técnicas (CONICET), and Universidad de Buenos Aires Científica y Tecnológica for financial support.

This work was supported by the Deutsche Forschungsgemeinschaft Centre for Molecular Physiology of the Brain (DFG CMPB), Cluster of Excellence 171 of the CMPB, in Göttingen, and the Max Planck Society (Toxic Protein Conformation project). M.J.R. was the recipient of fellowship support from the DFG CMPB and a doctoral fellowship from CONICET.

REFERENCES

1. Dohm, C. P., P. Kermer, and M. Bähr. 2008. Aggregopathy in neurodegenerative diseases: mechanisms and therapeutic implication. *Neurodegener. Dis.* 5:321–338.
2. Uversky, V. N. 2008. α-Synuclein misfolding and neurodegenerative diseases. *Curr. Protein Pept. Sci.* 9:507–540.
3. Uversky, V. N. 2010. Mysterious oligomerization of the amyloidogenic proteins. *FEBS J.* 277:2940–2953.
4. Stefani, M. 2010. Protein aggregation diseases: toxicity of soluble prefibrillar aggregates and their clinical significance. *Methods Mol. Biol.* 648:25–41.
5. Morris, A. M., M. A. Watzky, and R. G. Finke. 2009. Protein aggregation kinetics, mechanism, and curve-fitting: a review of the literature. *Biochim. Biophys. Acta.* 1794:375–397.
6. Malkus, K. A., E. Tsika, and H. Ischiropoulos. 2009. Oxidative modifications, mitochondrial dysfunction, and impaired protein degradation in Parkinson's disease: how neurons are lost in the Bermuda triangle. *Mol. Neurodegener.* 4:24.
7. Seshadri, S., K. A. Oberg, and V. N. Uversky. 2009. Mechanisms and consequences of protein aggregation: the role of folding intermediates. *Curr. Protein Pept. Sci.* 10:456–463.
8. Fauerbach, J. A., S. Yushchenko, …, E. A. Jares-Erijman. 2012. Supramolecular non-amyloid intermediates in the early stages of α-synuclein aggregation. *Biophys. J.* 102:1127–1136.
9. van Raaij, M. E., I. M. Segers-Nolten, and V. Subramaniam. 2006. Quantitative morphological analysis reveals ultrastructural diversity of amyloid fibrils from α-synuclein mutants. *Biophys. J.* 91:L96–L98.
10. Hoyer, W., D. Cherny, …, T. M. Jovin. 2004. Rapid self-assembly of α-synuclein observed by *in situ* atomic force microscopy. *J. Mol. Biol.* 340:127–139.
11. Sweers, K., K. van der Werf, …, V. Subramaniam. 2011. Nanomechanical properties of α-synuclein amyloid fibrils: a comparative study by nanoindentation, harmonic force microscopy, and Peakforce QNM. *Nanoscale Res. Lett.* 6:270.
12. Munishkina, L. A., and A. L. Fink. 2007. Fluorescence as a method to reveal structures and membrane-interactions of amyloidogenic proteins. *Biochim. Biophys. Acta.* 1768:1862–1885.
13. Bertoncini, C. W., and M. S. Celej. 2011. Small molecule fluorescent probes for the detection of amyloid self-assembly *in vitro* and *in vivo*. *Curr. Protein Pept. Sci.* 12:205–220.
14. Lindgren, M., and P. Hammarström. 2010. Amyloid oligomers: spectroscopic characterization of amyloidogenic protein states. *FEBS J.* 277:1380–1388.
15. Kaminski Schierle, G. S., C. W. Bertoncini, …, C. F. Kaminski. 2011. A FRET sensor for non-invasive imaging of amyloid formation *in vivo*. *Chem. Phys. Chem.* 12:673–680.
16. van Ham, T. J., A. Esposito, …, C. W. Bertoncini. 2010. Towards multiparametric fluorescent imaging of amyloid formation: studies of a YFP model of α-synuclein aggregation. *J. Mol. Biol.* 395:627–642.
17. Roberti, M. J., C. W. Bertoncini, …, T. M. Jovin. 2007. Fluorescence imaging of amyloid formation in living cells by a functional, tetracysteine-tagged α-synuclein. *Nat. Methods.* 4:345–351.
18. Thirunavukkuarasu, S., E. A. Jares-Erijman, and T. M. Jovin. 2008. Multiparametric fluorescence detection of early stages in the amyloid protein aggregation of pyrene-labeled α-synuclein. *J. Mol. Biol.* 378:1064–1073.
19. Roberti, M. J., M. Morgan, …, E. A. Jares-Erijman. 2009. Quantum dots as ultrasensitive nanoactuators and sensors of amyloid aggregation in live cells. *J. Am. Chem. Soc.* 131:8102–8107.
20. Yushchenko, D. A., J. A. Fauerbach, …, T. M. Jovin. 2010. Fluorescent ratiometric MFC probe sensitive to early stages of α-synuclein aggregation. *J. Am. Chem. Soc.* 132:7860–7861.
21. Roberti, M. J., L. Giordano, …, E. A. Jares-Erijman. 2011. FRET imaging by k(t)/k(f). *Chem. Phys. Chem.* 12:563–566.
22. Roberti, M. J., T. M. Jovin, and E. A. Jares-Erijman. 2011. Confocal fluorescence anisotropy and FRAP imaging of α-synuclein amyloid aggregates in living cells. *PLoS ONE.* 6:e23338.
23. Hell, S. W. 2007. Far-field optical nanoscopy. *Science.* 316:1153–1158.
24. Hell, S. W. 2009. Microscopy and its focal switch. *Nat. Methods.* 6:24–32.
25. Patterson, G., M. Davidson, …, J. Lippincott-Schwartz. 2010. Superresolution imaging using single-molecule localization. *Annu. Rev. Phys. Chem.* 61:345–367.
26. Betzig, E., G. H. Patterson, …, H. F. Hess. 2006. Imaging intracellular fluorescent proteins at nanometer resolution. *Science.* 313:1642–1645.
27. Rust, M. J., M. Bates, and X. Zhuang. 2006. Sub-diffraction-limit imaging by stochastic optical reconstruction microscopy (STORM). *Nat. Methods.* 3:793–795.

28. Fölling, J., M. Bossi, …, S. W. Hell. 2008. Fluorescence nanoscopy by ground-state depletion and single-molecule return. *Nat. Methods.* 5:943–945.

29. Fernández-Suárez, M., and A. Y. Ting. 2008. Fluorescent probes for super-resolution imaging in living cells. *Nat. Rev. Mol. Cell Biol.* 9:929–943.

30. Outeiro, T. F., P. Putcha, …, P. J. McLean. 2008. Formation of toxic oligomeric α-synuclein species in living cells. *PLoS One.* 3:e1867.

31. Thompson, M. A., J. S. Biteen, …, W. E. Moerner. 2010. Molecules and methods for super-resolution imaging. *Methods Enzymol.* 475:27–59.

32. Vogelsang, J., T. Cordes, …, P. Tinnefeld. 2010. Intrinsically resolution enhancing probes for confocal microscopy. *Nano Lett.* 10:672–679.

33. Fölling, J., V. Belov, …, S. W. Hell. 2007. Photochromic rhodamines provide nanoscopy with optical sectioning. *Angew. Chem. Int. Ed. Engl.* 46:6266–6270.

34. Bossi, M., J. Fölling, …, S. W. Hell. 2008. Multicolor far-field fluorescence nanoscopy through isolated detection of distinct molecular species. *Nano Lett.* 8:2463–2468.

35. Belov, V. N., M. L. Bossi, …, S. W. Hell. 2009. Rhodamine spiroamides for multicolor single-molecule switching fluorescent nanoscopy. *Chemistry.* 15:10762–10776.

36. Bates, M., B. Huang, …, X. Zhuang. 2007. Multicolor super-resolution imaging with photo-switchable fluorescent probes. *Science.* 317:1749–1753.

37. Vogelsang, J., C. Steinhauer, …, P. Tinnefeld. 2010. Make them blink: probes for super-resolution microscopy. *Chem. Phys. Chem.* 11:2475–2490.

38. Egner, A., C. Geisler, …, S. W. Hell. 2007. Fluorescence nanoscopy in whole cells by asynchronous localization of photoswitching emitters. *Biophys. J.* 93:3285–3290.

39. Heise, H., W. Hoyer, …, M. Baldus. 2005. Molecular-level secondary structure, polymorphism, and dynamics of full-length α-synuclein fibrils studied by solid-state NMR. *Proc. Natl. Acad. Sci. USA.* 102:15871–15876.

40. Fernández, C. O., W. Hoyer, …, T. M. Jovin. 2004. NMR of α-synuclein-polyamine complexes elucidates the mechanism and kinetics of induced aggregation. *EMBO J.* 23:2039–2046.

41. Antony, T., W. Hoyer, …, V. Subramaniam. 2003. Cellular polyamines promote the aggregation of α-synuclein. *J. Biol. Chem.* 278:3235–3240.

42. Ahmad, M. F., T. Ramakrishna, …, ChM. Rao. 2006. Fibrillogenic and non-fibrillogenic ensembles of SDS-bound human α-synuclein. *J. Mol. Biol.* 364:1061–1072.

43. Ban, T., K. Morigaki, …, Y. Goto. 2006. Real-time and single fibril observation of the formation of amyloid β spherulitic structures. *J. Biol. Chem.* 281:33677–33683.

44. Fölling, J., V. Belov, …, S. W. Hell. 2008. Fluorescence nanoscopy with optical sectioning by two-photon induced molecular switching using continuous-wave lasers. *Chem. Phys. Chem.* 9:321–326.

45. Andersen, C. B., H. Yagi, …, C. Rischel. 2009. Branching in amyloid fibril growth. *Biophys. J.* 96:1529–1536.

46. Ban, T., K. Yamaguchi, and Y. Goto. 2006. Direct observation of amyloid fibril growth, propagation, and adaptation. *Acc. Chem. Res.* 39:663–670.

47. Kaminski Schierle, G. S., S. van de Linde, …, C. F. Kaminski. 2011. *In situ* measurements of the formation and morphology of intracellular β-amyloid fibrils by super-resolution fluorescence imaging. *J. Am. Chem. Soc.* 133:12902–12905.

48. Duim, W. C., B. Chen, …, W. E. Moerner. 2011. Sub-diffraction imaging of huntingtin protein aggregates by fluorescence blink-microscopy and atomic force microscopy. *Chem. Phys. Chem.* 12:2387–2390.

49. Lee, H. J., and S. J. Lee. 2002. Characterization of cytoplasmic α-synuclein aggregates. Fibril formation is tightly linked to the inclusion-forming process in cells. *J. Biol. Chem.* 277:48976–48983.

50. Ding, T. T., S. J. Lee, …, P. T. Lansbury, Jr. 2002. Annular α-synuclein protofibrils are produced when spherical protofibrils are incubated in solution or bound to brain-derived membranes. *Biochemistry.* 41:10209–10217.

51. Xu, S. H. 2007. Aggregation drives "misfolding" in protein amyloid fiber formation. *Amyloid.* 14:119–131.

52. Engelender, S., Z. Kaminsky, …, C. A. Ross. 1999. Synphilin-1 associates with α-synuclein and promotes the formation of cytosolic inclusions. *Nat. Genet.* 22:110–114.

53. Kramer, M. L., and W. J. Schulz-Schaeffer. 2007. Presynaptic α-synuclein aggregates, not Lewy bodies, cause neurodegeneration in dementia with Lewy bodies. *J. Neurosci.* 27:1405–1410.

54. Scott, D. A., I. Tabarean, …, S. Roy. 2010. A pathologic cascade leading to synaptic dysfunction in α-synuclein-induced neurodegeneration. *J. Neurosci.* 30:8083–8095.

55. Jones, S. A., S. H. Shim, …, X. Zhuang. 2011. Fast, three-dimensional super-resolution imaging of live cells. *Nat. Methods.* 8:499–508.

56. Spagnuolo, C. C., R. J. Vermeij, and E. A. Jares-Erijman. 2006. Improved photostable FRET-competent biarsenical-tetracysteine probes based on fluorinated fluoresceins. *J. Am. Chem. Soc.* 128: 12040–12041.